Accepted paper for Trans. Inst. Mats. Finish. TIMF 1064 01 Apr. 2016

Composite, multi-layer and three-dimensional substrate supported tin based electrodeposits from methanesulfonic acid

F.C. Walsh *, [1] and C.T.J. Low [1, +]

[1] Electrochemical Engineering Laboratory and Materials Engineering Research Group, Engineering Sciences, University of Southampton, Highfield, Southampton, SO17 1BJ, UK.

[+] Present address: WMG, Energy Innovation Centre, University of Warwick, Coventry, CV4 7AL, UK.

*Corresponding author. Email: F.C. Walsh@soton.ac.uk
Telephone number: +44 (0)23 8059 8752; Fax number: +44 (0)23 8059 8754.

Abstract

Tin and tin-alloy deposits enjoy many applications in the electronics, tribology and engineering industries with potential applications as electrodes for lithium batteries and as electrocatalyst coatings. Methanesulfonic acid has become a favoured electrolyte due to its environmental benefits and ability to offer a vehicle for many metal alloy, conductive polymer and composite coatings. A number of emergent uses require less common compositions or structures of alloy, polymer or composite deposits. This paper concisely provides diverse examples of modern tin-containing deposits from aqueous methanesulfonic acid, including Sn-Cu alloys having a very wide composition together with a wide range of colours (golden yellow-dark brown) and surface finishes, a Sn-Cu composite deposit containing ceramic, protonated titanium oxide nanotubes for batteries, a tin-copper-bismuth ternary alloy and tin deposits supported on an inert reticulated vitreous carbon or carbon felt substrate to provide a porous, 3-dimensional tin surface for electrocatalysis and batteries. The importance of controlled current distribution and electrode/electrolyte movement are illustrated by the use of the rotating disc electrode (RDE), rotating cylinder electrode (RCE) and rotating cylinder Hull (RCH) cell.

Keywords: bronze deposits, carbon felt, reticulated vitreous carbon, rotating electrodes, tin-copper alloys.

1. Introduction

Recent reviews have considered single metal tin [1] and tin-copper alloy electroplating [2]. This paper considers speciality tin deposits from a methanesulfonic acid bath, deposition of other single metals and Sn-Cu alloys which have been studied recently in our laboratory.

The attractions of methanesulfonic acid (MSA) electrolytes include their versatility, ability to dissolve many metals, 'green' credentials compared to traditional electrolytes [3] and versatility in surface finishing. The extremely wide range of coatings and surface finishes possible from such electrolytes (single metals, alloys, ceramics, polymers and composites) by electroplating, electrophoresis and anodising has recently been profiled [4].

The deposition of tin and its alloys has traditionally been important as corrosion protective coatings, particularly for foodstuffs and in the electronics industry [1,2]. More recently, electrochemically produced nanostructured, multilayer and composite films have become important in rapidly-developing applications such as wear and corrosion resistant surfaces [5] or in speciality batteries and electrocatalysts [6, 7]. This paper briefly explores the potential for tin-based electrodeposits in developing application areas. Use is made of a controlled flow rotating cylinder cathode Hull cell, as described elsewhere [8-12].

The following section provides a summary of the electrochemical response of tin and tin-copper electrodeposition in MSA electrolytes, with an emphasis on the role of a commercially sourced perfluorinated cationic surfactant DuPont ForaFac®1098. Readers are directed to previous research studies for further details [12-14].

Electrodeposition of tin and copper occurred by a two electron reduction of their divalent cations:

$$Sn^{2+} + 2e^- \rightarrow Sn \qquad E^o = -0.14\ V\ vs.\ SHE \tag{1}$$

$$Cu^{2+} + 2e^- \rightarrow Cu \qquad E^o = +0.34\ V\ vs.\ SHE \tag{2}$$

The standard electrode potentials have been stated versus the standard hydrogen electrode, the value for tin being significantly less noble than that for copper

Electrodeposition of tin

In the absence or presence of the surfactant, electrodeposition of tin onto a copper substrate initiates at approximately –0.44 V *vs.* Ag|AgCl [12] and took place though a 3-D instantaneous nucleation with diffusion-controlled growth [13]. Under static conditions, a single reduction peak (Sn^{2+} to Sn) and oxidation peak (Sn to Sn^{2+}) are observed in the cyclic voltammetry with or without the addition of surfactant. However, a single limiting current density is observed in the surfactant-free electrolytes under a controlled flow condition (via rotating electrodes). The limiting current density appeared as peaks and valleys in the presence of surfactant; implying possible adsorption and desorption mechanisms. All tin deposited in the charge transfer and limiting current region were matte finish with a compact and uniform coverage. At a more negative potential, needle-like dendritic deposits were obtained in surfactant-free electrolytes and rod-like deposits were observed at high current density in surfactant-containing electrolytes.

Electrodeposition of tin-copper alloys

In the presence of surfactant, the potential for copper charge transfer controlled deposition was shifted to a more electronegative potential and was brought back to a more electropositive potential with increasing copper ion concentration in the electrolytes. This means that both 'normal' deposition (Cu deposited at a more electropositive potential than Sn) and 'anomalous' deposition (Sn deposited at a more electropositive potential than Cu) could be achieved. Golden yellow coloured bronze deposits, containing 70–80% wt Cu and 20–30% wt Sn were obtained.

When Sn was deposited preferentially, the Cu content of the alloy was typically in the range 3–9% wt. Surface microstructures of the deposits are compact when deposited in the mixed controlled region, but irregular and cracks appeared in deposits obtained under the mass transport control; roughened and powdery deposits were obtained at a potential more negative than that of hydrogen evolution:

$$2H^+ + 2e^- = H_2 \qquad E^o = 0 \text{ V } vs. \text{ SHE} \qquad (3)$$

2. Experimental details

2.1 Chemicals and materials

A summary is given here; further details of experimental conditions are available elsewhere [16]. The substrate chosen for most experiments was 316L stainless steel. This was wet-polished down to 0.1 μm using silicon carbide papers then alumina on a Selvyt polishing cloth (Buehler). Studies on a carbon foam substrate used RVC, grade 100 ppi (pores per linear inch) having a nominal electrode area per unit electrode volume of 66 cm^2 cm^{-3} [17], which was supplied by the Electrosynthesis Company Inc, USA, and the carbon felt was 3 mm thick GFA grade Sigrafelt®, supplied by the SGL Group, Germany. All substrates were ultrasonically cleaned in alcohol then rinsed in ultrapure (reverse osmosis and deionised, <1 μS cm^{-1} electrolytic conductivity) water before use.

2.2 Voltammetry

A Pyrex glass, 3-electrode cell was used with a working electrolyte compartment of ca. 100 cm^3. The 2 cm^2 platinum mesh counter electrode was separated from the working electrode by a Nafion® 117 proton exchange membrane. The electrolyte in the working electrode compartment

was purged by a fast nitrogen stream for 20 minutes before use and a nitrogen blanket was maintained over the solution. All experiments were carried out at 25±1 ^{o}C.

2.3 Electrodeposition

For tin electrodeposition, the electrolyte contained 0.05 mol dm^{-3} $SnSO_4$. For tin-copper deposition, the bath contained 0.1 mol dm^{-3} $CuSO_4$ and 0.05 mol dm^{-3} $SnSO_4$. Both electrolytes contained 0.01 mol dm^{-3} hydroquinone and 0.01 % vol. surfactant ForaFac® 1098 (Dupont) in 2.3 mol dm^{-3} MSA. All experiments were performed at 25±1 ^{o}C with continuous agitation of the 150 cm^3 electrolyte by a circular disc electrode (3 mm radius, 0.28 cm^2 surface area) rotating at ca. 1000 rpm. All experiments were carried out at 25±1 ^{o}C. Experimental details of electrodeposition using a rotating cylinder Hull cell were similar to those reported previously [16, 18].

3. Results

3.1 Cyclic voltammetry of Cu-Sn deposition

Cyclic voltammetry of tin-copper alloy deposition and anodic stripping from a static 316L stainless steel disc substrate showed four distinct peaks associated with the reduction and oxidation of Cu(II)-Cu(0) and Sn(II)-Sn(0) redox couples, Figure 1a). The peak potentials of the tin-copper electrolytes remained unchanged compared with their individual electrolyte formulations. The cationic surfactant did not form complexes with soluble Cu(II) and Sn(II) ions; tin and copper could be co-deposited. Peak A is associated with the reduction of Sn(II) to Sn(0); Peak B represents the reduction of Cu(II) to Cu(0) and the current density was merged with that for tin; Peak C and D can be associated with the oxidation stripping of tin, copper and their alloys. Commonly, working electrode potential was measured versus a silver/silver chloride reference electrode ($E_{Ag/AgCl}$ = 0.222 V *vs.* SHE).

3.2 Electrodeposition of Cu-Sn alloys

Tin-copper alloys [14, 15, 18, 19] were deposited under controlled flow condition, using potentiostatic technique (via the rotating cylinder electrode) and galvanostatic technique (via the rotating cylinder Hull cell). The rotating cylinder Hull cell was used to deposit a controlled non-uniform distribution of tin-copper alloys along the cathode length. It showed that a wide range of tin content, 5 to 50% wt could be co-deposited with the copper, from 30 to 45% wt. tin content in the electrolyte, to produce dark-grey, light-brown or golden-yellow surface colour. The surface microstructure of the deposits was characterised using a scanning electron microscope and the metal composition of the alloy surface was measured using energy dispersive x-ray analysis.

At low current density, the tin-copper alloys contained predominantly copper; 20 to 35% wt tin had a golden yellow surface finish and 35 to 50% wt tin gave a light to dark brown appearance. The electrode rotation speed and stannous ion concentration showed no significant influence on the composition of tin-copper alloys. The current density region for golden-yellow surface finishes was lengthened with increasing stannous ion concentration in the electrolyte; for example, when stannous ion concentration increased from 0.03 to 0.06 mol dm^{-3}, this region was lengthened from 4.0 to 6.5 cm along the cathode; approximately 63% and increased in the region corresponding to a golden-yellow surface finish. The copper limiting current density was used as a guideline in choosing the applied current, such that tin-copper alloys with golden-yellow surface finishes were deposited using approximately 20 to 40% of the copper limiting current density [19].

Linear sweep voltammetry showed that tin can be preferentially deposited at a more positive potential than copper, this was achieved only from a low copper ion concentration, <0.1 mol dm^{-3} copper(II) in the tin-copper baths. From an electrolyte containing 0.02 mol dm^{-3} $CuSO_4$, 0.05 mol dm^{-3} $SnSO_4$, 0.005 mol dm^{-3} (12.5% vol.) methanesulfonic acid, hydroquinone and 0.01% vol.

surfactant; Sn-Cu alloys containing 3 to 9% wt copper were deposited onto the rotating cylinder Hull cell cathode. At the lower current density region along the cathode, tin-copper alloys deposits showed uniform surface microstructure and a medium silvery grey surface finish while nodular tin-copper alloys were deposited in the high current density region. This is in agreement with the linear sweep voltammetry that showed copper began to codeposit at a more negative potential once initial deposition of tin had occurred.

3.3 Corrosion resistance of Sn, Cu and Sn-Cu deposits

Single metal and alloy deposits were obtained at a constant potential, −0.5 V *vs.* Ag|AgCl for tin and −0.4 V *vs.* Ag|AgCl for the tin-copper alloy. The Na_2SO_4 electrolyte was deoxygenated with a fast stream of nitrogen gas sparged through the electrolyte for 10 minutes and a nitrogen gas blanket was maintained over the electrolyte during measurements to minimise interference from oxygen reduction. Figure 2 shows the Tafel (current density as a function of electrode potential) plots for tin, copper and tin-copper deposits in 0.5 mol dm^{-3} Na_2SO_4 at 25 ^oC. Under these conditions, the anodic and cathodic reactions are likely to be dissolution of tin as stannous ions or copper as cupric ions together with hydrogen evolution at the tin or tin-copper deposits.

The corrosion potentials were −0.44 *V vs.* Ag|AgCl for tin, −0.002 V *vs.* Ag|AgCl for copper and +0.032 V *vs.* Ag|AgCl for the tin-copper alloy (35% wt Sn, 65% wt Cu), indicating the copper and Sn-Cu deposits to be more noble than the tin. Extrapolation of the Tafel regions allowed the corrosion current densities to be estimated as 0.02 mA cm^{-2} for tin, 0.10 mA cm^{-2} for copper and 0.05 mA cm^{-2} for the tin-copper alloy, indicating the mean corrosion rate under these conditions to be in the order: Cu > Sn-Cu> Sn.

3.4. Composite deposition of tin-copper alloy containing titanium oxide nanoparticles

Figure 3a) shows the structure of nanotubular protonated titanate ($H_2Ti_3O_7$) particles. The titanate nanotubes were synthesised by an alkaline hydrothermal method as described elsewhere [20]. This extends the existing titanate-polymer and metal-particle composites such as titanate nanotubes in electrodeposited polypyrrole [21] and in nickel coatings [22]. Figure 3b) shows the surface microstructure of a copper composite deposit containing titania nanoparticles. The 10 μm thick coating, which was compact and adherent to the copper substrate, was deposited from the same electrolyte described previously but containing 20 g dm^{-3} of dispersed nanotubular titanates. No visible surface pores or cracks were observed. As in our previous work on electrodeposited Ni containing nanotubular titanates, [22] a good distribution of the particles over the surface was evident and some particles can be seen protruding from the top surface. This widens the range of available particles, from nanometre up to micron size, in metal-matrix electrodeposited composites [22, 23].

3.5. Multi-layered deposits

Figure 4 shows a cross-sectional view of alternating multi-layers of tin (lighter area, 1 μm thickness) and copper (darker area, 10 μm thickness) deposited from methanesulfonic acid electrolytes containing the perfluorinated cationic surfactant, using a dual bath system. The individual Sn and Cu layers were deposited using the similar electrolyte compositions and deposition conditions as those described above. Sn layer was deposited at −0.5 V *vs.* Ag|AgCl for 5 minutes, while the copper layer deposited at −0.4 V *vs.* Ag|AgCl for 10 minutes onto a 316L stainless steel rotating cylinder electrode at ca. 1000 rpm. Electrodeposition of alternating tin and copper multilayers from a single methanesulfonic acid bath containing both tin and copper would also be possible by potentiostatic pulsing or galvanostatic pulsing coupled with the judicious use of complexant/surfactant additives.

3.6 Controlled deposition of 3-dimensional structure copper and tin deposits

High surface area electrodes are important in applications such as electrochemical detectors, batteries, and fuel cells. The increased surface area can provide an enhanced current density. Figure 5 shows three-dimensional copper and tin deposits obtained in the high current density region along the cathode of the rotating cylinder Hull cell. The microstructures were deposited at an applied current 100 mA for 10 min, using similar electrolyte composition stated in the experimental details. The presence of perfluorinated cationic surfactant in the methanesulfonic acid electrolytes has affected the surface microstructure of deposits at high current density at potentials more negative than those seen in the complete mass transport controlled region. By controlled evolution of hydrogen bubbles during copper deposition, self-supported metallic foam of copper deposit containing a complex network of interconnected pores between multiparticle clusters can be obtained, see Figure 5a). Three-dimensional tin deposits containing vertically stand rods can also be obtained via inhibition of the hydrogen evolution reaction. This approach can be used to create copper metallic foams and tin 'porcupine' electrodes which are well-supported, mechanically robust and chemically stable (Figure 5b). Such structures might prove interesting for energy conversion devices which often require high surface area electrode structures, such as batteries and supercapacitors [24].

3.7. Sn-Cu-Bi ternary alloy deposits

While a number of binary tin alloy electroplating baths have been considered, ternary tin alloy electrodeposits are unusual [25]. An electrolyte was prepared containing 15% vol. methanesulfonic acid 0.01 mol dm^{-3} hydroquinone, 0.02% vol. cationic surfactant and equal $SnSO_4$ $CuSO_4$ and Bi_2O_3 concentrations of 0.01 mol dm^{-3}. A rotating cylinder Hull cell involving a 316L stainless steel rotating cylinder cathode at 1000 rpm was used and a current of 600 mA was applied for 15 minutes. Figure 6 shows the surface content and microstructure of the tin-copper-bismuth alloy deposits; 2% wt. bismuth was obtained in the low current density region and 50% wt. bismuth in

the high current density region. For 4Sn46Cu50Bi, Figure 6a) shows the surface microstructure and Figure 6b) the EDX analysis. For 7Sn–91Cu–2Bi. Figure 6c) shows the surface microstructure and Figure 6d) the EDX analysis. Such deposits may find use in the electronics industry as lead-free solders [26].

3.6. High surface area electrode materials

Figure 7 shows tin-copper alloy deposits on reticulated vitreous carbon, RVC and on a porous carbon felt. These substrates can offer good chemical, heat resistance and the open structure allows a low resistance to fluid flow. High porosity and increased specific surface area can be advantageous as electrode materials for fuel cells and batteries such that the effect of pulverization may be significantly lowered, leading to improved performance and long-term stability. Other coatings recently applied on RVC have included Cu [27], polypyrrole [28] and finely divided platinum [29]. Figure 7a) shows the surface microstructure and Figure 7b) the surface alloy content, corresponding to a deposit of 4Sn46Cu50Bi. Figure 7b) shows a cross-sectional image of the tin-copper alloy on the carbon felt substrate shown in Figure 7c). Figure 7d) shows the uniformly deposited alloy on the surface of a single string of the carbon felt. Investigations can be carried out to understand the arrangement of deposits (layer, columnar) grown from the substrate. More advanced studies could be carried out on deposition of composite and multilayers coatings on both the reticulated vitreous carbon (RVC) and carbon felt surface. The former support material has the benefits of flexibility and high surface area porosity but is limited by a microporosity which changes with compression as well as a surface chemistry which is easily altered by adsorption [30]. The RVC structure presents a rigid, open macropore network which provides a low pressure drop for electrolyte flow but suffers from being brittle in applications such as batteries and fuel cells [29].

Electrodeposition of tin-copper alloys a) on a porous, 100 ppi reticulated vitreous carbon (volumetric porosity of 97%) support; b) cross-sectional view of the RVC; (c) GFA5 (Sigrafelt)

carbon felt [30] (volumetric porosity of 68%); (d) a higher magnification view of deposits from b), showing single strands of the felt having a typical diameter 5-10 μm.

4. Conclusions

1. A wide variety of tin coatings can be electrodeposited from MSA baths, by suitable control of the electrolyte composition and operating conditions, including bath composition and current density together with adequate electrolyte agitation/cathode movement.

2. A wide range of tin and tin alloy deposit composition and morphology are possible by suitable choice of bath composition (including suitable additives) and controlled flow.

3. Increasingly diverse tin-ceramic particle deposits increase the available range of composite coatings facilitated by coupling electrodeposition of the metal or alloy with convection-assisted electrophoretic deposition of included particles available for electronics and tribology applications.

4. Multilayers of copper and tin have been electrodeposited using alternating tin and copper baths; this opens the convenience of potential pulsing from a single bath.

5. Two very different porous, 3-dimensional graphite felt and reticulated vitreous carbon supports have been electrodeposited with tin. The resulting structures may prove useful in extending the electrical charge capacity of flow batteries and the power density of liquid fuel cells.

5. Further work

Further research and development studies are recommended in the following areas:

a) more advanced studies on incorporation of corrosion inhibitors and various additives to enhance the corrosion resistance of copper, tin and their alloy deposits.

b) the influence of surfactants on the incorporation of nanoparticles into single metal tin and copper; alloys, gradient distributional and multi-layers of tin-copper deposits; investigations

should be focused on understanding the interactive effects of electrode geometry and operating parameters such as current density, electrode rotation speed, electrolyte composition and temperature on the coatings.

c) the adsorption and desorption of perfluorinated cationic surfactants during deposition requires a more detailed, mechanistic study.

d) further tailoring of nanostructured deposits might be realised by control of process parameters such as electrode potential, electrolyte composition (especially electrocrystallisation additives) and relative movement between the cathode and electrolyte.

e) the influence of various cations on tin-copper alloy baths and the possible suppression of surface roughening of these deposits by nickel and cobalt ions.

f) development of multilayers involving 3 or more metals, different alloy compositions and composites, such as progressive heat transfer and bearing layers.

g) ambitious gradient and diagnostic coatings for corrosion and tribology applications [31], such as those for rapid bed-in bearings and those requiring tell-tale progressive wear signals.

Acknowledgements

The studies in this paper have been informed by the 2007 PhD thesis of CTJL at the University of Southampton. The authors gratefully acknowledge early contributions to this work via funding from the Research Institute for Industry in Engineering Sciences at Southampton University and a current Green Tribology EPSRC grant with Prof R. Wood and Dr J.A. Wharton in our tribology centre, nCATS (EP/J001023/1).

References

1. F.C. Walsh, C.T.J. Low, A review of developments in the electrodeposition of tin, *Surf. Coat. Technol*., 2016, **288**, 79.

2. F.C. Walsh, C.T.J. Low, A review of developments in the electrodeposition of copper-tin (bronze) alloys, in preparation, 2016.

3. M.D. Gernon, M. Wu, T. Buszta, P. Janney, Environmental benefits of methanesulfonic acid: Comparative properties and advantages, *Green Chemistry*, 1999, **1**, 127.

4. F.C. Walsh, C. Ponce de León, Versatile electrochemical coatings and surface layers from aqueous methanesulfonic acid, *Surf. Coat. Techno*l., 2014, **259**, 676.

5. C.T.J. Low, F.C. Walsh, "Electroplated multifunctional and nanostructured coatings", Ch. 7 in R.J.K. Wood, (Ed), Multifunctional Materials for Tribological Applications, Pan Stanford, 2014, pp 227.

6. F.C. Walsh, C. Ponce de León, D.V. Bavykin, C.T.J. Low, S.C. Wang, The formation of nanostructured surfaces by electrochemical techniques: a range of emerging surface finishes. Part 1. Achieving nanostructured surfaces by electrochemical techniques, *Trans. Inst. Mats. Finish*., 2015, **93**, 229.

7. F.C. Walsh, C. Ponce de León, D.V. Bavykin, C.T.J. Low, S.C. Wang, The formation of nanostructured surfaces by electrochemical techniques: a range of emerging surface finishes. Part 2. Examples of nanostructured surfaces by plating and anodizing with their applications, *Trans. Inst. Mats. Finish*., 2015, **93**, 241.

8. C. Madore, D. Landolt, The rotating cylinder Hull cell: design and application, *Plating and Surf. Finish*., 1993, **80**, 73.

9. C. Madore, M. Matlosz, D. Landolt, Experimental investigation of the primary and secondary current distribution in a rotating cylinder Hull cell, *J. Appl. Electrochem*., 1992, **22**, 1155.

10. C. Madore, A.C. West, M. Matlosz, D. Landolt, Design considerations for a cylindrical Hull cell with forced convection, *Electrochim. Acta*, 1992, **3**7, 69.

11. C.T.J. Low, E.P.L. Roberts, F.C. Walsh, Numerical simulation of the current, potential and concentration distributions along a rotating cylinder Hull cell cathode, *Electrochim. Acta*, 2007, **52**, 3831.

12. C.T.J. Low, F.C. Walsh, The stability of an acidic tin methanesulfonate electrolyte in the presence of a hydroquinone antioxidant, *Electrochim. Acta*, 2008, **53**, 5280.

13. C.T.J. Low, C. Kerr, C. Ponce-de-León, F.C. Walsh, Electrodeposition of tin at static and rotating copper disk electrodes: voltammetry, nucleation and morphology, Ch. 13 in U.S. Mohanty, (Ed), Electrodeposition: Properties, Processes and Applications, Nova Publishers, New York, 2012, p 283.

14. C.T.J. Low, F.C. Walsh, The influence of a perfluorinated cationic surfactant on the electrodeposition of tin from an aqueous methanesulfonic acid, *J. Electroanal. Chem*., 2008, **615**, 91.

15. C.T.J. Low, F.C. Walsh, Linear sweep voltammetry of the electrodeposition of copper from a methanesulfonic acid bath containing a perfluorinated cationic surfactant, *Surf. Coat. Technol*., 2008, **202**, 3050.

16 C.T.J. Low, Rotating electrodes for the electrodeposition of tin and tin-copper alloys, PhD thesis, University of Southampton, 2007.

17. J.M. Friedrich, C. Ponce-de-León, G.W. Reade, F.C. Walsh, Reticulated vitreous carbon as an electrode material, *J. Electroanal. Chem.*, 2003, **561**, 203.

18. C.T.J. Low, F.C. Walsh, Electrodeposition of tin, copper and tin-copper alloys from a methanesulfonic acid electrolyte containing a perfluorocarbon cationic surfactant, *Surf. Coat. Technol.*, 2008, **202**, 1339.

19. C.T.J. Low, F.C. Walsh, Normal and anomalous electrodeposition of tin-copper coatings from a methanesulfonic acid bath containing a perfluorinated cationic surfactant, *Trans. Inst. Met. Finish.*, 2008, **86**, 315.

20. D.V. Bavykin, F.C. Walsh, Titanate and Titania Nanotubes: Synthesis, Properties and Applications, Royal Society of Chemistry Nanoscience and Nanotechnology Monograph, 2009.

21. A.N. Kulak, D.V. Bavykin, C. Ponce de León, J. Zekonyte, F.C. Walsh, Electrodeposition of polypyrrole-titanate nanotube composite coatings and their corrosion resistance, *Electrochim. Acta*, 2011, **58**, 1323.

22. C.T.J. Low, R.G.A. Wills, F.C. Walsh, Electrodeposition of composite coatings containing nanoparticles in a metal deposit, *Surf. Coat. Technol*., 2006, **201**, 371.

23. F.C. Walsh, C. Ponce de León, A review of the electrodeposition of metal matrix composite coatings by inclusion of particles in a metal layer: an established and diversifying coatings technology", *Trans. Inst. Mats. Finish.*, 2014, **92**, 83.

24. G. Wang, L. Zhang, J. Zhang, A review of electrode materials for electrochemical supercapacitors, *Chem. Soc. Rev.,* 2012, **41**, 797.

25. M. Jordan, The Electrodeposition of Tin and its Alloys, E.G. Leuze, Saulgau, Germany, 1995.

26. Y. Goh, A.S.M.A. Haseeb, M. Faizul, M. Sabri, Effects of hydroquinone and gelatin on the electrodeposition of Sn–Bi Low temperature Pb-free solder, *Electrochim. Acta*, 2013, **90**, 265.

27. R. Tangirala, C.T.J. Low, C. Ponce-de-León, S.A. Campbell, F.C. Walsh, Copper deposition at a segmented reticulated vitreous carbon cathode in a Hull cell, *Trans. Inst. Met. Finish*., 2010, **88**, 84.

28. Y. Yuan, S. Kim, Polypyrrole-coated reticulated vitreous carbon as anode in microbial fuel cell for higher energy output, *Bull. Korean Chem. Soc*. 2008, **29**, 168.

29. A. Kulak, S. Williams, I. Merino-Jiménez, C. Ponce de León, F.C. Walsh, Improvements in the direct borohydride fuel cell using three-dimensional electrodes, *Catalysis Today*, 2011, **70**, 149.

30. M.J. Watt-Smith, H. Al-Fetlawi, P. Ridley, R.G.A. Wills, A.A. Shah, F.C. Walsh., The importance of operational variables, mathematical modelling and electrolyte monitoring to the performance of a vanadium redox flow battery, *J. Chem. Technol. Biotechnol.*, 2013, **88**, 126.

31. Y. He, S.C. Wang, F.C. Walsh, W.S. Li, L. Heb, P.A.S. Reed, The monitoring of coating health by *in-situ* luminescent layers, *RSC Advances*, 2015, **5**, 42965.

Figure captions

Figure 1. a) Cyclic voltammetry at a static 316L stainless steel disc electrode in The electrolyte compositions are 0.1 mol dm^{-3} $CuSO_4$, 0.05 mol dm^{-3} $SnSO_4$, 0.01 mol dm^{-3} methanesulfonic acid (2.3 mol dm^{-3} CH_3SO_3H, pH < 1), 0.01 mol dm^{-3} hydroquinone, $C_6H_4(OH)_2$ and 0.01 % vol. DuPont™ ForaFac® 1098 at 25 °C and a linear potential sweep rate of 16 mV s^{-1}, showing four distinct peaks associated with the reduction and oxidation of Cu(II)/Cu(0) and Sn(II)/Sn(0) redox couples.

Figure 2. Tafel plots for tin, copper and tin-copper alloy deposits in deaerated 0.5 mol dm^{-3} Na_2SO_4 at 298 K. The deposits were obtained at a constant potential; −0.5 V *vs.* Ag|AgCl for tin and −0.4 V *vs.* Ag|AgCl for copper and the tin-copper alloy. The Na_2SO_4 electrolyte was deoxygenated with nitrogen gas for 10 minutes and a nitrogen blanket was maintained over the electrolyte during measurements.

Figure 3. The structure of nanotubular titanium oxide particles; a) clusters of deposited titanate nanotubes on the copper support surface and (b) the surface microstructure of a copper composite coating containing titanate nanotubes.

Figure 4. A cross-sectional view of alternating tin (lighter area, 1 μm thickness) and 10 μm copper layers deposited from methanesulfonic acid electrolytes containing a perfluorinated cationic surfactant. Sn layer was deposited at −0.5 V *vs.* Ag|AgCl for 5 minutes, while the copper layer deposited at −0.4 V *vs.* Ag|AgCl for 10 minutes onto a 316L stainless steel rotating cylinder electrode at ca. 1000 rpm.

Figure 5. Controlled electrodeposition of three-dimensional metal deposit structures in the presence of a cationic perfluorinated surfactant. (a) Porous, 3-D copper deposit and

b) projectile growths from a tin deposit. Similar electrolyte compositions to those for copper and tin deposition in Figure 1 were used. The microstructures were deposited at an applied current 100 mA for 10 min onto a 0.6 cm diameter, 8 cm long 316L stainless steel rotating cylinder electrode, rotating at 1000 rev min^{-1}. Images were taken from the high current density region of the rotating cylinder Hull cell, ca. 3.5 cm from the high current density end.

Figure 6. Tin-copper-bismuth ternary alloy deposits. (a) surface microstructure and (b) surface alloy containing 4% Sn, 46% Cu and 50%wt bismuth; (c) surface microstructure and (d) elemental content of the surface alloy content containing 7% Sn, 91% Cu and 2%wt Bi. A rotating cylinder Hull cell involving a 316L stainless steel rotating cylinder cathode at 1000 rpm was used and a current of 600 mA was applied for 15 minutes.

Figure 7. Electrodeposition of tin-copper alloys a) on a porous, 100 ppi reticulated vitreous carbon (97% volumetric porosity) support; b) cross-sectional view of the RVC; (c) GFA5 (Sigrafelt) carbon felt (volumetric porosity of 68%); (d) a higher magnification view of deposits from b), showing single strands of the felt having a typical diameter 5-10 μm.

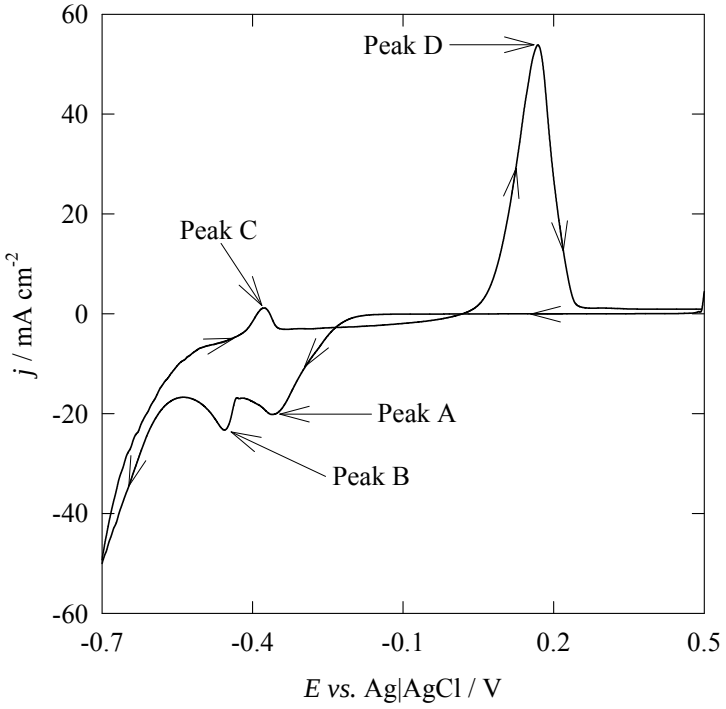
Peak D
Peak C
Peak A
Peak B
60
40
20
0
-20
-40
-60
-0.7
-0.4
-0.1
0.2
0.5
j / mA cm-2
E vs. Ag|AgCl / V

Figure 1

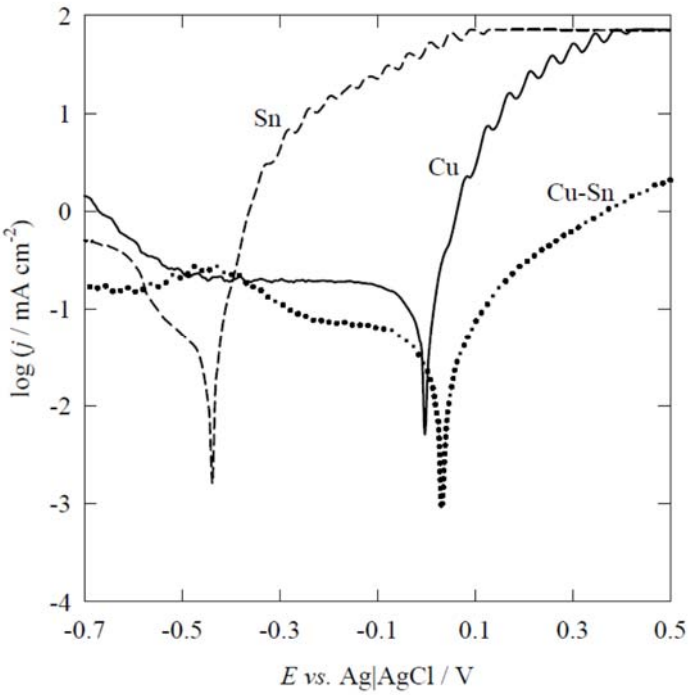

Figure 2

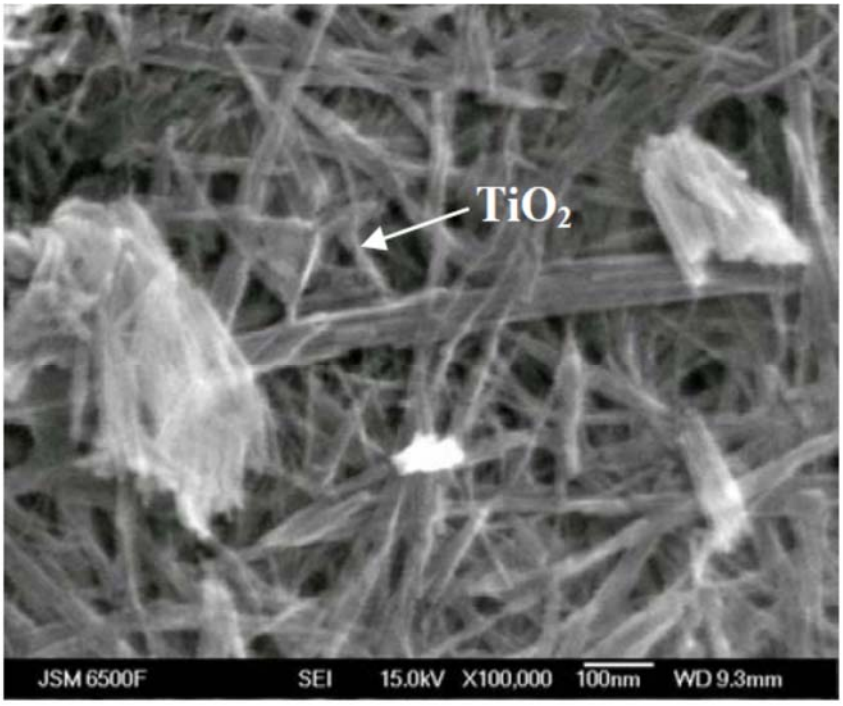
TiO2
JSM 6500F SEI 15.0kV X100,000 100nm WD 9.3mm

a)

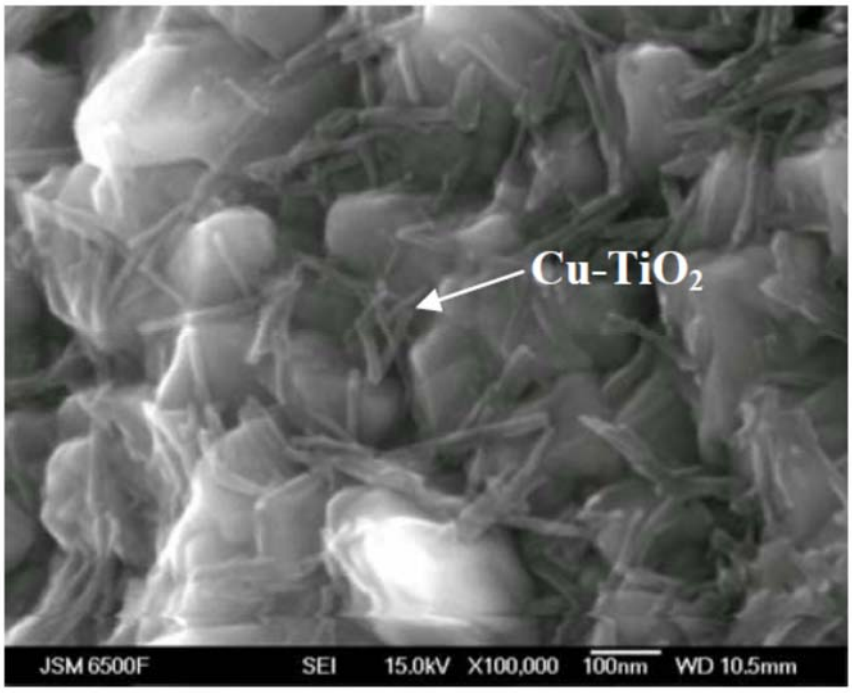
Cu-TiO2
JSM 6500F SEI 15.0kV X100,000 100nm WD 10.5mm

b)

Figure 3

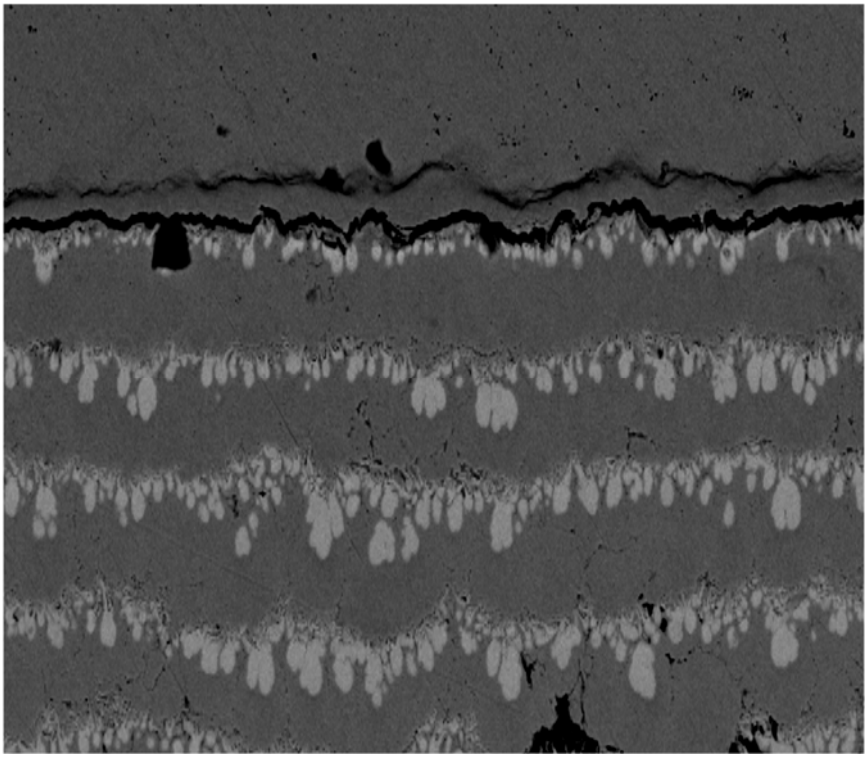

20 μm

Figure 4

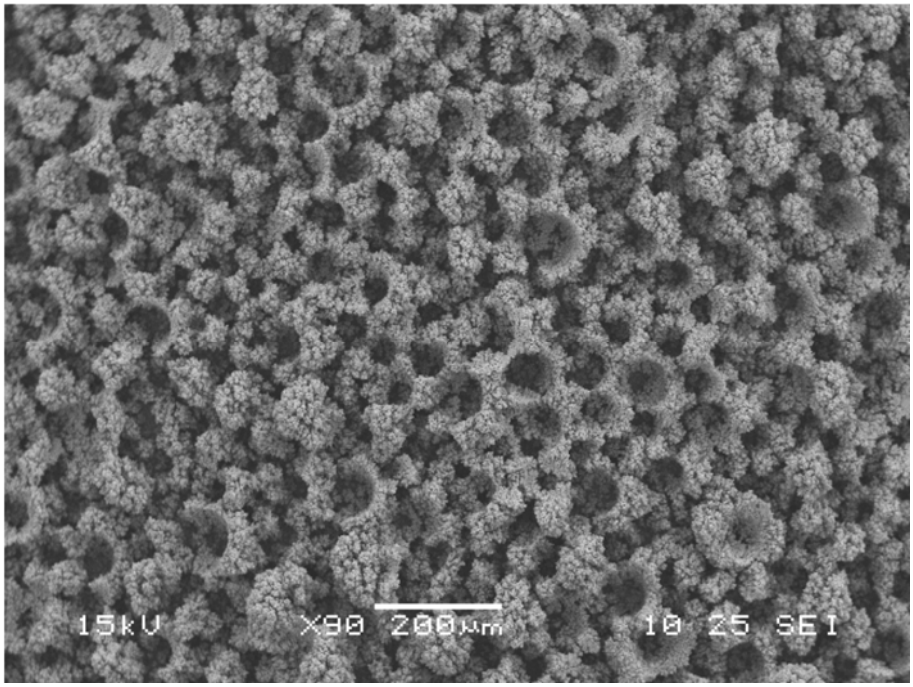

a)

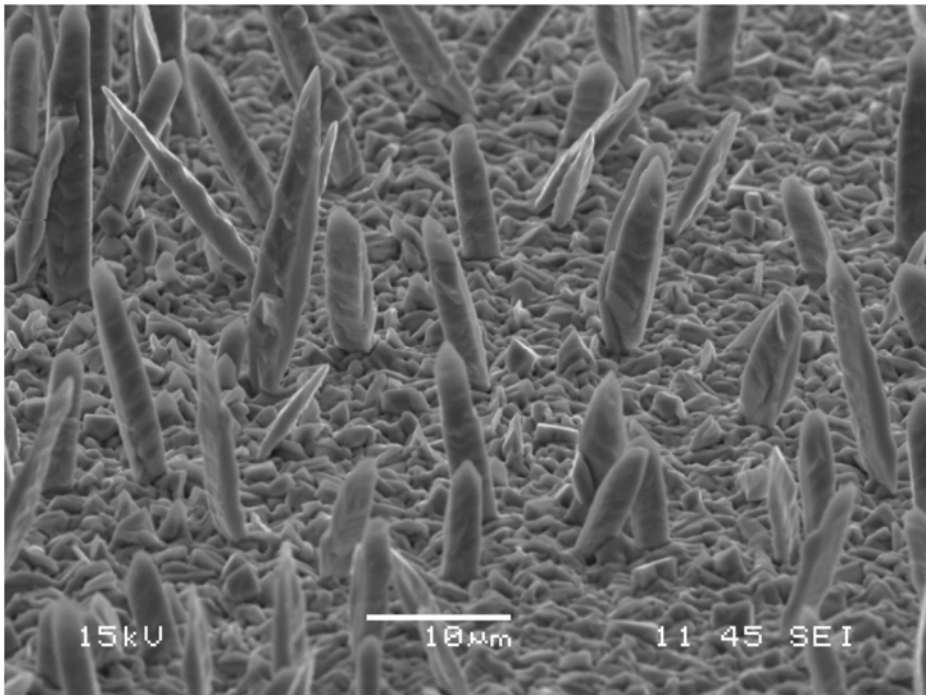

b)

Figure 5

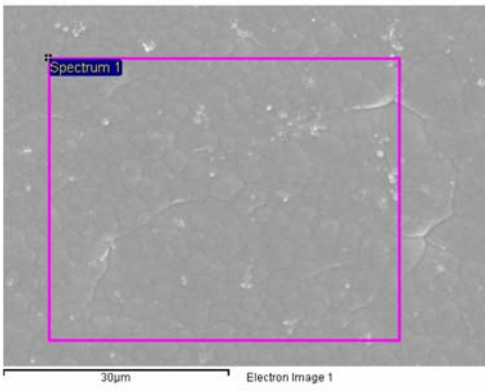

a)

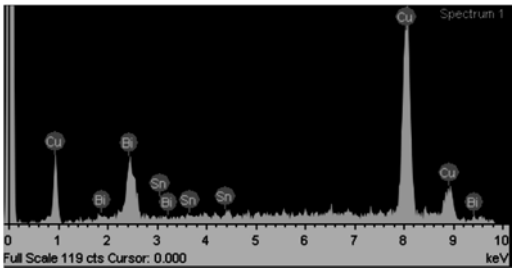

b)

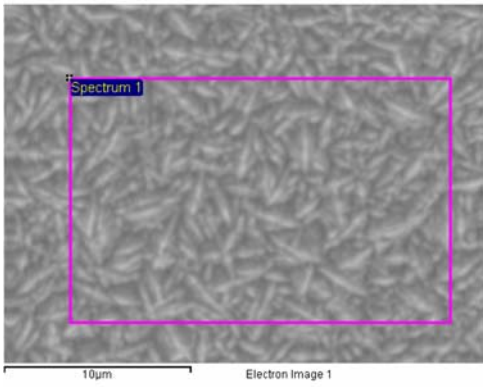

c)

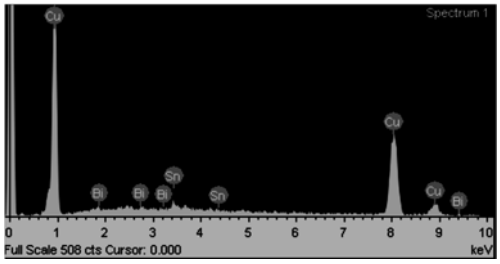

d)

Figure 6

Deposits on 100 ppi reticulated vitreous

200 µm

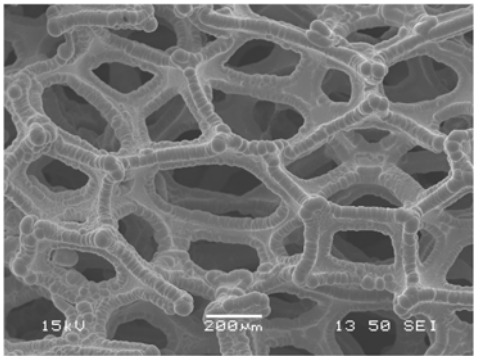

a)

Cross-sectional of deposit on 100 ppi reticulated vitreous

5 µm

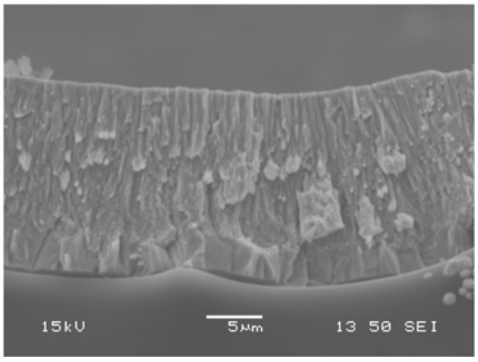

b)

Carbon felt (68% volumetric porosity)

200 µm

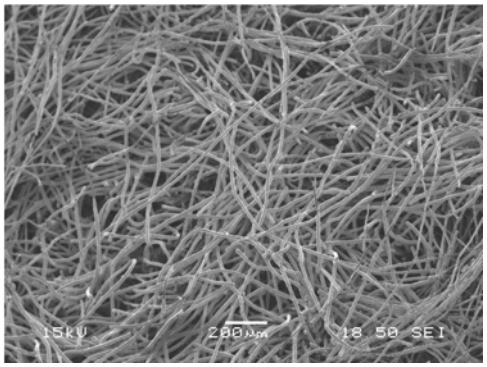

c)

Deposits on the carbon felt

10 µm

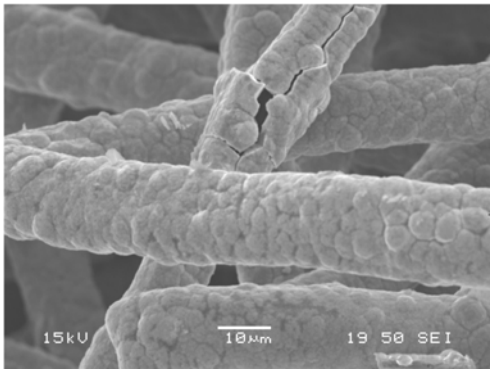

d)

Figure 7